MOLECULAR
METABOLISM

Regulation of lymphatic function and injury by nitrosative stress in obese mice

Sonia Rehal [1], Raghu P. Kataru [1], Geoffrey E. Hespe, Jung Eun Baik, Hyeung Ju Park, Catherine Ly, JinYeon Shin, Babak J. Mehrara*

ABSTRACT

Objective: Obesity results in lymphatic dysfunction, but the cellular mechanisms that mediate this effect remain largely unknown. Previous studies in obese mice have shown that inducible nitric oxide synthase-expressing (iNOS+) inflammatory cells accumulate around lymphatic vessels. In the current study, we therefore tested the hypothesis that increased expression of iNOS results in nitrosative stress and injury to the lymphatic endothelial cells (LECs). In addition, we tested the hypothesis that lymphatic injury, independent of obesity, can modulate glucose and lipid metabolism.

Methods: We compared the metabolic changes and lymphatic function of wild-type and iNOS knockout mice fed a normal chow or high-fat diet for 16 weeks. To corroborate our *in vivo* findings, we analyzed the effects of reactive nitrogen species on isolated LECs. Finally, using a genetically engineered mouse model that allows partial ablation of the lymphatic system, we studied the effects of acute lymphatic injury on glucose and lipid metabolism in lean mice.

Results: The mesenteric lymphatic vessels of obese wild-type animals were dilated, leaky, and surrounded by iNOS+ inflammatory cells with resulting increased accumulation of reactive nitrogen species when compared with lean wild-type or obese iNOS knockout animals. These changes in obese wild-type mice were associated with systemic glucose and lipid abnormalities, as well as decreased mesenteric LEC expression of lymphatic-specific genes, including vascular endothelial growth factor receptor 3 (VEGFR-3) and antioxidant genes as compared with lean wild-type or obese iNOS knockout animals. *In vitro* experiments demonstrated that isolated LECs were more sensitive to reactive nitrogen species than blood endothelial cells, and that this sensitivity was ameliorated by antioxidant therapies. Finally, using mice in which the lymphatics were specifically ablated using diphtheria toxin, we found that the interaction between metabolic abnormalities caused by obesity and lymphatic dysfunction is bidirectional. Targeted partial ablation of mesenteric lymphatic channels of lean mice resulted in increased accumulation of iNOS+ inflammatory cells and increased reactive nitrogen species. Lymphatic ablation also caused marked abnormalities in insulin sensitivity, serum glucose and insulin concentrations, expression of insulin-sensitive genes, lipid metabolism, and significantly increased systemic and mesenteric white adipose tissue (M-WAT) inflammatory responses.

Conclusions: Our studies suggest that increased iNOS production in obese animals plays a key role in regulating lymphatic injury by increasing nitrosative stress. In addition, our studies suggest that obesity-induced lymphatic injury may amplify metabolic abnormalities by increasing systemic and local inflammatory responses and regulating insulin sensitivity. These findings suggest that manipulation of the lymphatic system may represent a novel means of treating metabolic abnormalities associated with obesity.

1. INTRODUCTION

Obesity results in impaired lymphatic function, and lymphatic abnormalities cause adipose deposition and obesity independent of dietary changes [1—5]. This reciprocal relationship suggests that obesity-induced lymphatic dysfunction may amplify the pathologic effects of obesity in a feed-forward manner, which likely contributes to the morbidity of obesity. Thus, understanding the cellular mechanisms that regulate this interaction has wide-ranging clinical relevance.

Several studies have shown that abnormalities in the lymphatic system can modulate adipose deposition and metabolic function. For example, mice with genetic abnormalities of the lymphatic system develop adult-onset obesity and metabolic syndrome, even when fed a normal diet [5]. Abnormal adipose deposition in these models is regulated, at least in part, by fatty acid-mediated activation of adipocyte proliferation and differentiation and can be reversed by targeted treatments that restore normal lymphatic function [4]. Recent reports have highlighted the important role of mesenteric lymphatic vessels and intestinal villi lacteals in lipid chylomicron absorption. Mice with inactivating

mutations of the tyrosine kinase domain of vascular endothelial growth factor receptor 3 (VEGFR-3, Chy mice) have lymphatic developmental defects and impaired enterocyte triglyceride absorption [6]. Furthermore, zippering of the villi lymphatic vessels (lacteals) prevents chylomicron uptake and renders the mice resistant to diet-induced obesity [7]. Similarly, lymphatic injury resulting from surgical trauma or infection with parasites leads to lymphedema, a disease characterized by progressive fibroadipose tissue deposition [8,9]. The interaction between the lymphatic system and adipose tissue is unsurprising given their close physical contact: lymphatic vessels and lymph nodes are surrounded by adipose tissue, which serves as a nutrient depot [10].

More recent studies have shown that obesity markedly impairs lymphatic function. Obese patients have decreased clearance of macromolecules from adipose tissue as compared with lean controls, and in extreme cases, obese individuals spontaneously develop lymphedema in their lower extremities [11—13]. Decreased lymphatic function in obesity results from increased lymphatic leakiness, decreased collecting vessel pumping capacity, and architectural changes in the lymphatics and lymph nodes [2,3]. Importantly, obesity-mediated changes in the lymphatic system require abnormal adipose deposition or inflammation and are independent of dietary changes, as evidenced by the fact that mice with genetic resistance to diet-induced obesity do not develop lymphatic dysfunction even after prolonged exposure to high-fat diet [14].

Although the cellular mechanisms by which obesity induces lymphatic dysfunction remain largely unknown, several lines of evidence suggest that local adipose tissue inflammation is necessary. Obesity-induced lymphatic abnormalities are partially reversible through weight loss or aerobic exercise, and improved lymphatic function in these circumstances is associated with decreased infiltration of leukocytes and reduced expression of inflammatory cytokines in subcutaneous adipose tissue [14,15]. Further, pharmacological therapies that decrease inflammation improve lymphatic function in obese animals without altering adipose deposition, suggesting that local inflammatory reactions, rather than physical compression of lymphatic channels, in obesity play an important role in the pathology of obesity-induced lymphatic dysfunction. For example, topical treatment with tacrolimus, an interleukin (IL)-2 inhibitor that decreases T-cell proliferation and differentiation, decreases lymphatic leakiness and improves pumping only in the area where the treatment is applied, without affecting adipose hypertrophy or modulating systemic metabolic abnormalities [3].

Several inflammatory mechanisms have been proposed to underlie obesity-induced lymphatic dysfunction and resulting lymphatic vessel dilatation, leakiness, and impaired collecting vessel pumping. These putative mechanisms include (a) regulation of adipokine expression, (b) release of long-chain free fatty acids by necrotic adipocytes causing lymphatic endothelial cell (LEC) injury, and (c) increased expression of inducible nitric oxide synthase (iNOS) by inflammatory cells [3,14,16—18]. In fact, earlier reports revealed that high concentrations of NO inhibit lymphatic contraction frequency and amplitude [19—21] and impaired NO signaling causes abnormal lymphatic contractile function in mouse models of diabetes [22]. The expression of iNOS by inflammatory cells in the subcutaneous adipose tissue of obese mice is significantly increased as compared with controls, and these iNOS^{+} cells tend to cluster around lymphatic vessels [3]. In obese mice or mice with chemically induced intestinal inflammation, inhibition of iNOS using the small molecule 1400 W significantly increases lymphatic pumping and transport function and decreases perilymphatic inflammation [3,23,24]. In these conditions, increased

expression of iNOS is thought to increase nitric oxide (NO) concentration, disrupting endogenous gradients ordinarily regulated by endothelial nitric oxide synthase (eNOS). However, increased lymphatic leakiness and other abnormalities in lymphatic function suggest that increased NO production may have additional pathologic effects.

In the current study, we tested the hypothesis that increased iNOS expression results in lymphatic injury by causing nitrosative stress. This hypothesis is based on the observations that dermal LECs are sensitive to oxidative stress in wound healing [25] and that oxidative stress induces blood endothelial dysfunction in a number of pathologic settings via endothelial cell apoptosis and extracellular matrix changes [26]. In addition, we tested the hypothesis that lymphatic injury modulates obesity-induced insulin resistance using a transgenic mouse in which the lymphatic system can be ablated using diphtheria toxin. The findings presented herein demonstrate the central role of iNOS and NO production in obesity-induced impaired lymphatic function, as well as regulation of systemic inflammation and metabolism by the lymphatics. Overall, our results provide important evidence supporting the hypothesis that these abnormalities can activate a feed-forward mechanism that increases the pathophysiology of obesity.

2. MATERIALS AND METHODS

2.1. Animals
All experimental protocols were approved by the Institutional Animal Care and Use Committee at Memorial Sloan Kettering Cancer Center (MSK) and performed in accordance with MSK-approved guidelines. Male C57/BL6 mice (Jackson Laboratories, Bar Harbor, Maine) aged 7—12 weeks were used for all experiments and were kept in a light- and temperature-controlled environment. Age-matched mice were fed either a normal chow diet containing 13% kcal from fat (Purina PicoLab Rodent Diet 20, W.F. Fisher and Son) or a high-fat diet (HFD) containing 60% kcal from fat (Purina TestDiet 58Y1, W.F. Fisher and Son) for 16 weeks. All experiments on mice with HFD-induced obesity were performed on mice weighing at least 40 g.

2.2. Lymphatic ablation
Fms-related tyrosine kinase 4 (FLT4)-diphtheria toxin receptor (DTR) mice were generated and DTR expression activated using previously published protocols [27]. Briefly, FLT4-CreER[T2] mice (a gift from Sagrario Ortega at the Centro Nacional de Investigaciones Oncológicas [CNIO] of Spain) were crossed with human DTR-floxed C57BL/6 mice (C57BL/6-Gt (ROSA)26Sor[tm1(HBEGF)Awai]/J; The Jackson Laboratory). Mice were mated for multiple backcrosses and Cre/lox expression was confirmed using polymerase chain reaction (PCR). To avoid the fatality associated with tamoxifen administration in double homozygous mice [14], we backcrossed them with wild-type C57B6 mice to create double heterozygous mice (i.e., FLT4 cre^{+/−}/DTR Loxp^{+/−}), of which males were treated with a single injection of 100 ng of DT administered intraperitoneally. The survival rate among these animals, in contrast to the homozygous mice, was approximately 80%, thus enabling us to collect tissues for analysis 1 week following DT treatment. Mice that had lost weight or appeared ill were excluded.

2.3. Assessment of lymphatic function
Mesenteric lymphatic vessel leakage was assessed by oral gavage of BODIPY (C16) (Thermo Fisher Scientific, Waltham, MA) suspended in olive oil (20 mL/200 mL). The mesentery was prepared for ex vivo imaging 1 h post-gavage. Through a mid-abdominal incision, the terminal small intestinal loop was exposed onto sterile saline-soaked

gauze. A viewing window of the mesenteric arcade was visualized using an intravital fluorescent stereomicroscope (Lumar V12, Zeiss, Germany). Lipid leakage was assessed using ImageJ software by quantifying fluorescence outside of the lymphatic vessel lumen after color thresholding and masking for extra-luminal green fluorescence. Indocyanine green (ICG) lymphography was performed using our published technique [3]. Briefly, 15 μL of 0.15 mg/mL ICG (Sigma—Aldrich) was injected intradermally into the dorsal aspect of the hind limb and then visualized for hind limb collecting lymphatic vessels using an EVOS EMCCD camera (Life Technologies, Carlsbad, CA, USA) with an LEC light source (CoolLEC, Andover, UK). A Zeiss Lumar.V12 stereo microscope (Caliper Life Sciences, Hopington, MA, USA) was used to obtain video images. A region of interest on a fluorescent, pulsating popliteal lymphatic vessel was chosen and recorded over 15 min of time lapse imaging. Lymphatic vessel pulsations were calculated on a dominant collecting lymphatic vessel, and then the background intensity of fluorescence was subtracted. The pulsations are plotted over time. Each experiment was repeated in 4—5 animals per group.

Dendritic cell (DC) migration/uptake into LNs from the peripheral skin was measured by FITC painting assay [15]. The backs of mice were shaved and painted with 8% FITC (type I isomers; Sigma—Aldrich, St. Louis, MO) diluted in a 1:1 mixture of acetone and dibutylphthalate (Sigma—Aldrich). The DC content (FITC$^+$/CD11c$^+$/MHC-II^{high}) of draining LNs was analyzed by flow cytometry (LSR II flow cytometer; BD Biosciences, San Diego, CA). Each experiment was repeated in 4—5 animals per group.

2.4. Cell culture and in vitro assays

Human dermal LECs and human umbilical vein embryonic cells (HUVECs) were obtained from PromoCell (Heidelberg, Germany), cultured in EGM-MV2 media containing 5% fetal bovine serum (FBS), epidermal growth factor (EGF) (5 ng/mL), hydrocortisone (0.2 μg/mL), basic fibroblast growth factor (BFGF) (10 ng/mL), insulin-like growth factor (ILGF) (20 ng/mL), VEGF 165 (0.5 ng/mL), ascorbic acid (1 μg/mL), and penicillin-streptomycin (50 U/mL) (Invitrogen, Carlsbad, CA), and passaged every 48 h. Diethylenetriamine (DETA) NONOate was purchased from Cayman Chemicals (Ann Arbor, MI, USA) and N-acetyl cysteine (NAC) from Sigma (St. Louis, MO, USA). Cells were treated with drugs for 24 h unless otherwise specified. DETA NONOate is a stable donor of NO, activated by neutral pH, to release consistent levels of NO into media. Dose—response curves for apoptosis and cell proliferation were generated using doses of 25, 50, 100, 250, and 500 μM. Subsequent experiments were performed using 100 μM DETA NONOate. NAC was used at a well described antioxidant dose at a dose of 5 mM [28—30]. All in vitro experiments were repeated in triplicate.

For Matrigel tubule formation assays, 500 μL of media containing 100 μM (+/− DETA NONOate) and 50,000 cells were plated on a 24-well plate coated with Matrigel (Corning, Tewksbury, MA, USA) and incubated for 24 h. Tubule formation was imaged using phase contrast on an inverted microscope (Carl Zeiss, Oberkochen, Germany) and branch numbers counted using an Angiogenesis Analyzer (ImageJ).

Proliferation of LECs and HUVECs was measured using the CyQUANT assay (Thermo Fisher Scientific) as per manufacturer instructions. Briefly, frozen cell lysates were used in the assay, in which DNA of lysed cells binds to a strong fluorescent dye that emits at 485 nm. Emission was measured using a spectrophotometer (Tecan M200, Mannedorf, Switzerland).

Early and late apoptosis were measured using the Dead Cell Apoptosis kit (Thermo Fisher Scientific) according to kit protocol.

Early apoptosis, defined by the externalization of phosphatidylserines on the cell surface, was detected by Annexin V antibody (conjugated to FITC), and late apoptosis was measured using propidium iodide (PI). Samples were analyzed using an Attune NxT flow cytometer (Thermo Fisher). Each experiment was repeated in 4—5 cell passages.

2.5. Whole-mount immunofluorescence

Small intestinal mesenteries pinned on Sylgard-coated dishes (Dow Corning, Midland, MI) were fixed in 10% formalin for 2 h, washed with Dulbecco's phosphate-buffered saline (DPBS), permeabilized for 2 h with 0.3% Triton X- 100/PBS, and subsequently blocked with 1% bovine serum albumin (BSA) for 2 h. Tissues were then incubated with primary antibody overnight at 4 °C in 0.3% Triton X-100/PBS, followed by secondary antibody for 5 h, and lastly thorough washes with 0.3% Triton X-100/PBS. Primary antibodies were as follows: mouse anti-iNOS (BD Biosciences, San Diego, CA), rabbit anti-n-tyrosine (Bioss, Woburn, MA), hamster anti-podoplanin (Abcam, Cambridge, UK), goat LYVE-1 (R&D, Minneapolis, MN), rat anti-CD45 (Abcam). Tissues were dehydrated in increasing concentrations of ethanol (50, 70, 90, and 100%) for 5 min each, then optically cleared using methyl salicylate for 5—10 min until transparent. Mesenteries were spread onto cover slides and mounted with methyl salicylate. Whole mounts were imaged using an inverted fluorescent microscope (Leica Microsystems, Germany). Each experiment was repeated on 4—5 mice.

2.6. Peroxynitrite measurement

Serum from mice was collected via cardiac puncture and analyzed for peroxynitrite and nitrate formation using the Griess reagent-based (Thermo Fisher Scientific) colorimetric (diazotization of nitrites) assay [31] per recommended protocol. The experiment was performed using 4—5 mice per group.

2.7. LEC permeability assay

LEC monolayer permeability was assessed using the transwell permeability assay. Briefly, LECs were seeded onto 6.4 mm wide, 0.4 μm transwells (Sigma) at a density of 1×10^5 cells/mL and treated for 24 h with EGM-V2 media (Invitrogen) alone, supplemented with DETA NONOate (100 μM), with 5 mM NAC, or DETA NONOate and NAC in combination. FITC-labeled BSA (10 mg/mL) leakage across the monolayer was measured using a fluorescent spectrophotometer (Tecan), at 485 nm. Each experiment was repeated in 4—5 replicates per group.

2.8. qPCR

Gene expression in cell lysates or LECs sorted from mesenteric lymph nodes (mLNs), pooled from 4 to 5 mice per experiment) was measured by qPCR. MLN single-cell suspensions were created by mechanical dissociation followed by enzymatic digestion with DNase I, dispase II, collagenase D, and collagenase IV (Roche Diagnostics, Indianapolis, IN), from which LECs were sorted (podoplanin$^+$/CD31$^+$/CD45$^-$) directly into lysis buffer (Qiagen, Hilden, Germany). RNA isolation was performed using RNeasy Mini and Micro kits for cell lysates and mLN LECs, respectively (Qiagen). cDNA was generated using Maxima H Minus cDNA Synthesis Master Mix and dsDNase (Thermo Fisher Scientific) using 8 μL of isolated RNA. qPCR was performed using QuantiTect SYBR Green PCR master mix (Qiagen) and pre-validated primer assays (Qiagen) using 1 μg of cDNA/reaction on a ViiA 7 Real-time PCR system (Thermo Fisher) per recommended protocol. After normalizing to β-actin expression, mRNA expression was measured as fold change using the ΔΔCt method. Samples with a

value > 30 for β-actin were excluded to ensure mRNA quality. Each analysis was performed in triplicate.

2.9. Enzyme-linked immunosorbent assay (ELISA)

Concentrations of VEGFC, VEGFA, total/phospho insulin receptor substrate 1 (IRS-1) protein concentration, tumor necrosis factor alpha (TNFα), IL-1β (all from Thermo Fisher Scientific), interferon gamma (IFNγ), adiponectin, IL-6 (all from R&D systems), and leptin (Abcam) were measured in serum, visceral adipose tissue (VAT), subcutaneous adipose tissue (SAT), and liver homogenates by ELISA. Briefly, tissues were homogenized using a TissueRuptor (Qiagen) in T-PER tissue protein extraction reagent (Thermo Fisher) containing phosphatase and protease inhibitors (Thermo Fisher). Each assay used 50 μg of homogenate. ELISA was performed in duplicates was repeated in 4—5 animals per group.

2.10. Flow cytometry

Cells expressing CD45, CD31, podoplanin, iNOS, CD11b, and F4/80 from digested mesenteric tissues were analyzed by flow cytometry [14]. Briefly, mesenteric tissues were digested in dispase (0.8 mg/mL), collagenase (0.2 mg/mL), and DNAse I (0.1 mg/mL) at 37 °C for 30 min. Digested tissues were filtered and resuspended in 2% FBS/sodium azide solution in PBS, then stained with fluorophore-conjugated antibodies (BD Biosciences). Stained cells were analyzed using a LSR Fortessa flow cytometer (BD Biosciences) and FlowJo software (Tree Star). Each experiment was repeated in 4—5 animals per group.

2.11. Assessment of insulin resistance and serum metabolic analysis

Serum lipids and insulin and liver function were assayed by the Center of Comparative Medicine and Pathology at MSK. Insulin resistance was measured by the intraperitoneal glucose tolerance test (IPGTT). After 12-h fasted mice were administered glucose via IP injection (2 g/kg in a total volume of 200 μL), blood was collected for glucose monitoring (Contour blood glucose monitoring device, Bayer, Germany) from a distal tail nick at 15, 30, 60, 90, and 120 min after IP injection. Insulin tolerance test was performed by intraperitoneal injection of insulin (0.5 U/kg in 100 μL volume; Sigma Aldrich) to 4-h fasted mice and blood was collected for glucose measurement at 15, 30, 60, 90, and 120 min after injection. Insulin resistance was calculated using homeostatic model assessment (HOMA) by the following calculation: fasting insulin x fasting glucose/405 [32]. Each experiment was repeated in 4—5 animals per group.

2.12. Statistical analysis

Statistical analysis was performed using Prism (GraphPad Software, San Diego, CA). Unpaired Student's t test was used to compare differences between two groups, whereas one- or two-way analysis of variance (ANOVA) was utilized for multiple groups. Data are presented as mean ± SD unless otherwise noted, and $p < 0.05$ was considered significant.

3. RESULTS

3.1. iNOS mediates mesenteric lymphatic vessel dysfunction in obese mice

Global knockout of iNOS has been shown to reduce the severity of obesity-associated insulin sensitivity and metabolic abnormalities in mice [33]. To determine the role of iNOS in regulating lymphatic function, we compared the metabolic phenotypes of iNOS knockout (iNOS KO) and wild-type mice fed a high-fat diet for 16 weeks. Consistent with previous reports, we found no significant differences in weight gain, food consumption, or inguinal/reproductive fat pad weights between wild-type and iNOS KO mice fed a high-fat diet (Supplementary Figs. 1A—E). iNOS KO in obese mice significantly improved glucose sensitivity as reflected by glucose tolerance, decreased serum insulin, decreased insulin resistance according to homeostatic model assessment (HOMA-IR), increased GLUT4 mRNA expression, and decreased phosphorylation of insulin receptor substrate 1 (IRS-1) at S307 in adipose tissues (Supplementary Figs. 2A—E). However, we found no differences in serum lipid profiles, including total cholesterol, high-density lipoprotein (HDL), low-density lipoprotein (LDL), and triglycerides (Supplementary Figure 2F). Both wild-type obese and iNOS KO obese mice had significantly increased serum leptin as compared with lean mice, but this change was less severe in iNOS KO obese animals (Supplementary Figure 2G). Similarly, obesity resulted in decreased serum adiponectin in both wild-type obese and iNOS KO obese mice as compared with lean controls; however, this difference was more pronounced in iNOS KO animals (Supplementary Figure 2H). Taken together, our results are consistent with previous studies and show that loss of iNOS expression in obesity decreases insulin resistance and improves glucose homeostasis but does not affect serum lipid concentrations [33].

We have previously shown that iNOS expression is increased in the skin of obese mice and that iNOS-positive cells tend to cluster around lymphatic vessels. Importantly, we also demonstrated that pharmacologic inhibition of iNOS partially restores lymphatic pumping capacity in obese mice [3]. In the current study, ICG lymphography revealed that obesity severely impaired the skin collecting lymphatic pumping rate in wild-type but not iNOS KO mice (Figure 1A—B). Consistent with these changes, in wild-type mice, obesity almost completely eliminated migration of dendritic cells (DCs) to regional lymph nodes, while in iNOS KO mice, obesity reduced DC migration to a lesser degree (Figure 1C). Confirming our observations in cutaneous lymphatics, the mesenteric lymphatics of obese wild-type mice were nearly 3 times more dilated and nearly 2-fold leakier as compared with lean animals as indicated by imaging following oral gavage of a fluorescent cholesterol, BODIPY (Figure 1D—F). In contrast, obese iNOS KO mice had normal appearing non-leaky lymphatic channels (Figure 1D—F).

3.2. Obesity-induced iNOS generates reactive nitrogen species in mesenteric tissues and alters gene expression in lymphatic endothelial cells

In agreement with prior studies implicating iNOS in obesity-induced impairment of lymphatic function [3,14,17], we observed a profound increase in the number of iNOS-positive cells (Figure 2A—B) and in iNOS mRNA expression in the mesenteric tissues of obese mice as compared with lean controls (Figure 2C). Staining for vascular endothelial growth factor receptor 3 (VEGFR-3) to localize lymphatic channels also indicated significantly dilated lymphatic vessels in obese mice. High-magnification confocal images of mesenteric tissues from obese mice showed that iNOS$^+$ cells colocalized with CD11b$^+$ inflammatory cells (Figure 2D). Quantitative assessment of mesenteric tissues by flow cytometry also showed that nearly 95% of CD45$^+$/iNOS$^+$ cells are CD11b$^+$/F480$^+$, indicating that these are macrophage- or myeloid-derived cells. Our results show that only a minuscule fraction of CD45$^-$ cells (stromal/ECM cells) are iNOS$^+$ (Figure 2E).

Increased levels of iNOS lead to supra-physiological levels of NO, which in turn generate reactive nitrogen and oxygen species [34]. To evaluate the effects of iNOS-induced NO on mesenteric lymphatic
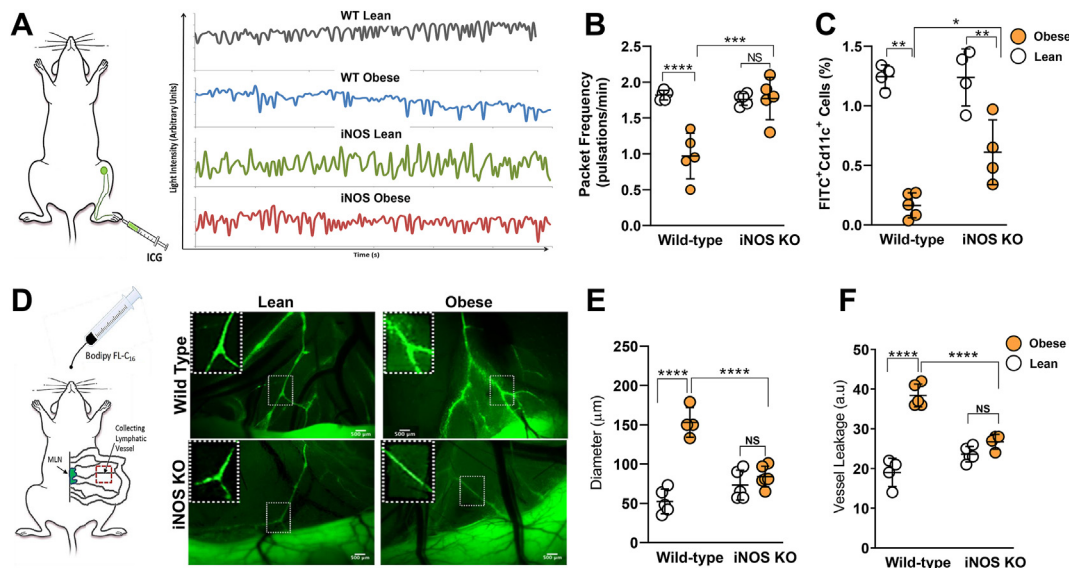
Figure 1: iNOS mediates mesenteric lymphatic vessel dysfunction in obese mice. All panels compare wild-type (WT) and iNOS KO lean and high-fat diet-induced obese mice. (A) Representative graphs of lymphatic vessel pulsation in popliteal lymphatic vessels measured using indocyanine green (ICG)-based lymphangiography. (B) Quantification of lymphatic vessel packet frequency. (C) Dendritic cell trafficking assessed using the FITC painting assay. (D) Visualization of collecting lymphatic vessels in mesenteric white adipose tissue (M-WAT) by oral gavage-administered BODIPY (FL-C16). Inset, 2x magnification showing dilated, leaky lymphatic vessels. Scale bar, 500 μm. (E) Quantification of M-WAT lymphatic vessel diameter and (F) BODIPY leakage into the extraluminal space. N = 5/group, mean ± SD, two-way ANOVA with Sidak multiple comparison test (*P < 0.05, **P < 0.01, ***P < 0.001 ****P < 0.0001).

vessels, we measured tissue and systemic levels of reactive nitrogen species, as well as nitration of tyrosine residues, the main NO-induced modification [35—37]. Immunostaining of mesenteric white adipose tissue (M-WAT) for nitrotyrosine (Figure 2F) demonstrated extensive tyrosine nitration in M-WAT in obese mice, primarily in the mesothelium, nearly 8-fold greater than in controls (Figure 2G). In contrast, although tyrosine nitration in obese iNOS KO mice was slightly increased as compared to lean control iNOS KOs, this difference did not reach statistical significance. These findings were confirmed by quantifying peroxynitrite production (nitrite and nitrate anions) using the Griess reaction (Figure 2G), which demonstrated a significant increase in peroxynitrite production in obese wild-type mice (6.6-fold as compared with lean controls; p < 0.0001) and no significant obesity-related change in iNOS KO mice.

To determine whether obesity alters mRNA expression of lymphatic-specific genes (VEGFR-3, podoplanin, Prox-1) and antioxidant enzymes in LECs, we sorted mesenteric lymph node LECs by flow cytometry and analyzed mRNA expression using real-time qPCR. LECs isolated from obese wild-type mice had decreased mRNA expression of VEGFR-3 and podoplanin as compared with LECs isolated from lean controls. In contrast, expression of VEGFR-3 was notably increased in obese iNOS KO mice as compared with lean iNOS KO controls. This finding suggests that NO either directly or indirectly regulates VEGFR-3 expression in LECs. Prox-1 expression did not differ in either genetic setting (Figure 2I—K). Expression of all 3 enzymes responsible for the majority of antioxidant activity in tissues, namely glutathione peroxidase (GPX), superoxide dismutase (SOD), and catalase (CAT) [38], was significantly decreased in LECs isolated from obese wild-type mice as compared with lean controls. In contrast, while the expression of all 3 antioxidant genes was decreased in obese iNOS knockout mice as compared with lean iNOS knockout controls, only the change in expression of SOD reached statistical significance (Figure 2L—N).

3.3. LECs are highly sensitive to nitrosative stress compared to HUVECs

To determine how nitrosative stress can modulate the function, survival, or differentiation of cultured LECs and vascular endothelial cells (HUVECs), we treated cultured cells with the stable NO donor, DETA NONOate (100 μM). DETA NONOate treatment did not significantly decrease the potential for HUVECs to form tubules in Matrigel. In contrast, the potential for tubule formation by LECs was severely compromised by this treatment (Figure 3A—B). We further assessed the DETA NONOate dose—response relationship of apoptosis and cell proliferation in LECs and HUVECs. DETA NONOate treatment led to dose-dependent decreases in LEC proliferation and increases in apoptosis. These effects reached statistical significance with doses as low as 100 μM. In contrast, none of the doses of DETA NONOate we tested had any effect on cultured HUVEC proliferation or apoptosis (Figure 3C—D). DETA NONOate treatment of LECs also reduced their barrier function, as assessed by transwell permeability assay using high molecular weight FITC dextran, which revealed significantly more leakage across the monolayer (Figure 3E).

To understand whether decreased LEC viability is transient or permanent, we cultured LECs with DETA NONOate for 1, 3, and 6 h, changed to fresh media without DETA NONOate, and assayed cell viability assay at 24 h. LEC viability decreased significantly by 6 h of DETA NONOate treatment and did not return to normal levels even after 24 h in fresh media, indicating that the decreased cellular viability is permanent (Supplementary Figs. 3A—B).

Consistent with our *in vivo* studies in obese mice, we found that treatment of LECs with DETA NONOate significantly decreased LEC mRNA expression of lymphatic genes (Prox-1, Podoplanin, VEGFR-3, LYVE1) and antioxidant genes (GPX and SOD) as compared with controls. To understand whether pro-lymphangiogenic growth factors can rescue the negative effects of DETA NONOate on LECs gene expression, we added VEGF-C to the culture media along with DETA

www.molecularmetabolism.com
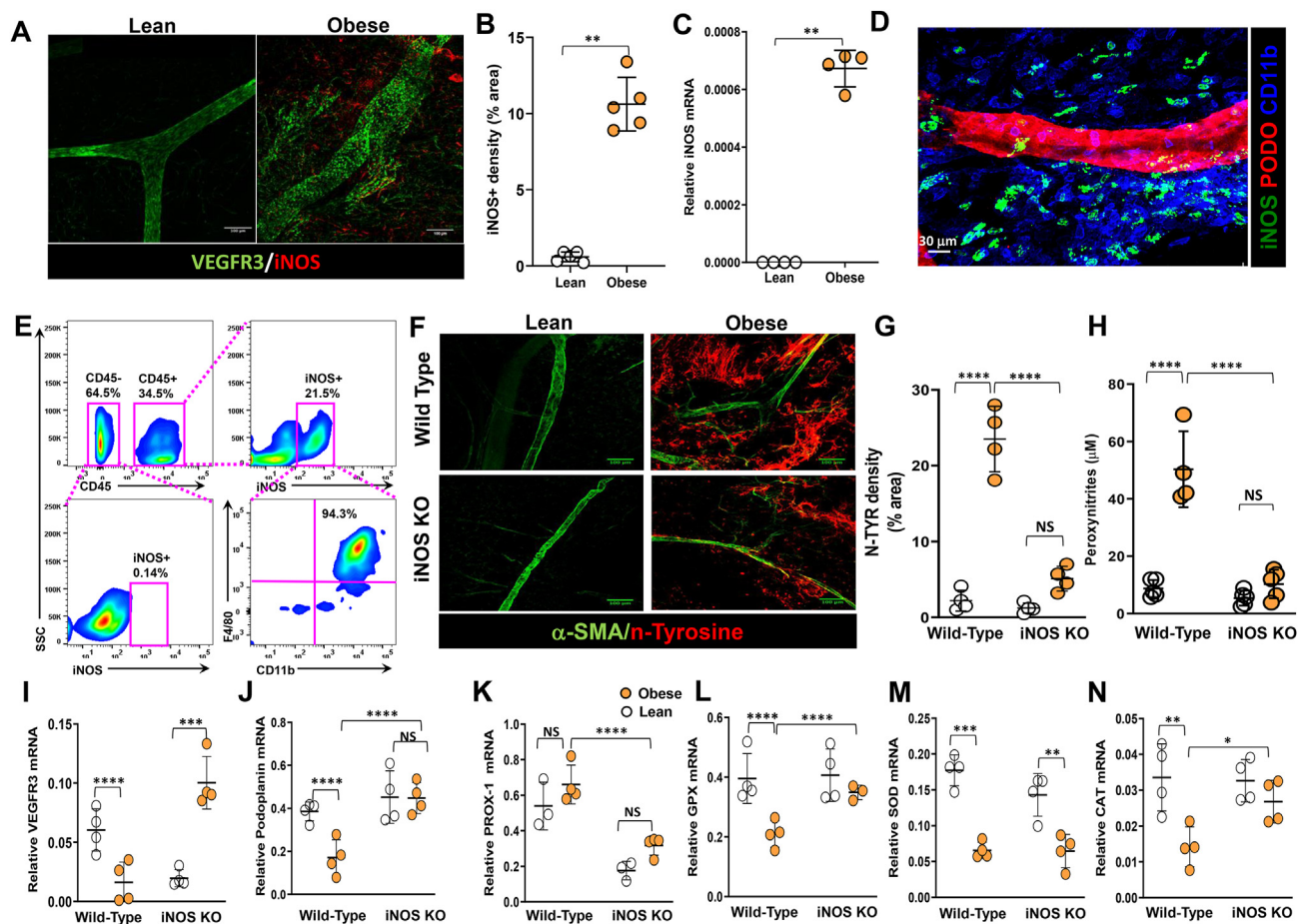
Figure 2: Obesity-induced iNOS generates reactive nitrogen species in mesenteric fat and iNOS alter gene expression in lymphatic endothelial cells. All panels compare WT and iNOS KO lean and high-fat diet-induced obese mice except panels D and E. (A) Representative microscopic images of M-WAT containing lymphatic vessels, immunostained for VEGFR-3 and iNOS (scale bar, 100 μm). (B) Quantification of fluorescent iNOS signal. (C) qPCR for iNOS gene expression, from M-WAT tissue, in NCD and HFD mice. (D) Representative microscopic images of M-WAT containing lymphatic vessels, immunostained for iNOS, podoplanin, and CD11b (scale bar, 30 μm). (E) Quantification of iNOS+ cells in M-WAT. Representative flow cytometry dot plots showing gating for CD45− and CD45+ cells among iNOS+ cells and CD45+/iNOS+ cells among CD11b/F480. (F) Representative microscopic images of M-WAT containing lymphatic vessels, immunostained for alpha smooth muscle actin (α-SMA) and nitrosylated tyrosine (n-tyrosine) (scale bar, 100 μm). (G) Quantification of fluorescent n-tyrosine signal. (H) Peroxynitrite production in serum. (I—N) qPCR quantification of gene expression in LECs from mesenteric lymph nodes for the lymphatic markers (I) vascular endothelial growth factor receptor 3 (VEGFR-3), (J) podoplanin, (K) PROX-1, and the antioxidant enzymes (L) glutathione peroxidase (GPX), (M) superoxide dismutase (SOD), and (N) catalase (CAT). N = 4—5/group, mean ± SD, two-way ANOVA with Sidak multiple comparison test. (**P < 0.01, **P < 0.01, ***P < 0.001, ****P < 0.0001).

NONOate. Adding VEGF-C to the culture media prevented the decrease in DETA NONOate-induced VEGFR-3 and GPX expression but did not rescue the expression of SOD or other LEC-specific or antioxidant genes (Figure 3F—K). We observed that DETA NONOate-induced downregulation of LEC genes is also permanent; removal of the NO donor for 24 h following 24-h treatment did not rescue gene expression changes (Supplementary Figs. 3C—G). The effects of DETA NONOate on tubule formation, apoptosis, and VEGFR-3 expression were reversed by the antioxidant N-acetylcysteine (Supplementary Figs. 4A—D), suggesting that these changes are related to reactive nitrogen species rather than non-specific toxicity. Together, our findings show that LEC proliferation, survival, and differentiation are highly sensitive to reactive nitrogen species.

3.4. Lymphatic injury causes insulin resistance and dyslipidemia
We next investigated the hypothesis that lymphatic dysfunction, independent of obesity, can lead to increased iNOS expression and metabolic abnormalities, such as insulin resistance or dyslipidemia.

To test this hypothesis, we used a Cre-lox mouse model in which the expression of the human diphtheria toxin receptor (DTR) is driven by FLT4, a lymphatic-specific promoter (FLT4-DTR) [39,40], upon tamoxifen-induced Cre-lox recombination. Injection of a single dose of diphtheria toxin (DT) 4—6 weeks later (after tamoxifen is cleared) leads to selective ablation of lymphatic vessels (both capillaries and collecting lymphatics), but not blood vessels, at the injection site, and systemic DT injection results in widespread lymphatic disruption, sepsis, and death within 24—48 h [39]. Administration of DT to healthy adult mice has no effect on other cell types (e.g., macrophages or other inflammatory cells) that express FLT4 in some pathologic circumstances (i.e., cancer or chronic inflammatory conditions) [41].

We first confirmed that a single intraperitoneal (IP) injection of DT in heterozygous FLT4-DTR mice (i.e., FLT4-cre+/−DTR+/−) results in loss of >50% of LECs in mesenteric tissues compared with littermate controls (Figure 4A; Supplementary Figure 5). Furthermore, DT injection either intradermally in the ear skin or intraperitoneally (IP) partially
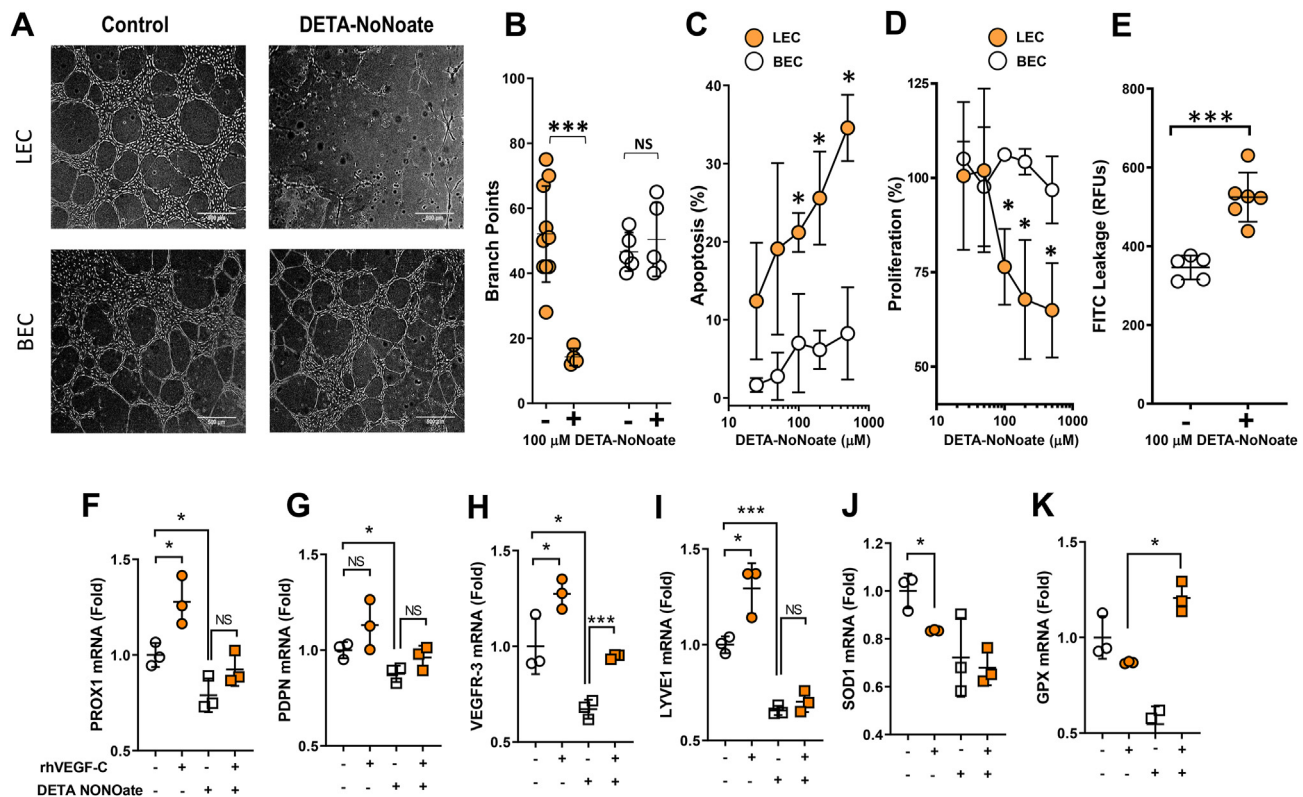
Figure 3: LECs are highly sensitive to nitrosative stress compared with HUVECs. (A) Representative phase-contrast images of Matrigel-based tubule formation by cultured human dermal LECs (LECs) and human umbilical vein endothelial cells (HUVECs) in the presence or absence of 100 μM DETA NONOate (scale bar, 500 μm). (B) Quantification of branch points generated in tubule formation assay by LECs and HUVECs in the presence or absence of 500 μM DETA NONOate. (C) Dose−response curves for late apoptosis in LECs and HUVECs with or without DETA NONOate. (D) Dose−response curves for the effects of DETA NONOate on cell proliferation in LECs and HUVECs. (E) Quantification of LEC monolayer leakage of high molecular weight FITC in the presence or absence of 100 μM DETA NONOate. (F−K) Gene expression via qPCR for the following lymphatic markers following treatment with or without DETA NONOate and VEGF-C: (F) PROX-1, (G) podoplanin, (H) VEGFR-3, (I) LYVE1, and the antioxidant enzymes (J) GPX and (K) SOD in LECs. A-E, N = 5/group; F−K, N = 3−4; mean ± SD, two-way ANOVA with Sidak multiple comparison test or unpaired Student's t test. (*P < 0.05, ***P < 0.001).

disrupted LYVE-1-stained lymphatic capillaries, causing a patchy, moth-eaten appearance in the ear skin and the intestinal lacteals, respectively. Lacteals in the villi and lymphatic capillaries in the lamina propria were disrupted in these animals (Supplementary Figs. 6A—B). Interestingly, we found that ablation of lymphatic vessels in skin and intestinal lymphatics increased the abundance of iNOS^{+} cells in the vicinity of injured lymphatic channels, suggesting that lymphatic damage causes inflammation similar to that in adipose tissue caused by obesity.

To study the effects of lymphatic ablation on systemic and adipose tissue metabolism, DT was administered IP to FLT4-cre^{+/−}DTR^{+/−} mice maintained on a normal chow diet. Mesenteric lymphatic ablation caused marked impairment of glucose metabolism within 1 week, as reflected by significantly increased serum glucose concentrations following IP glucose challenge compared with littermate controls (Figure 4B). Consistent with these findings, this treatment also markedly increased insulin resistance as reflected by significantly higher serum glucose concentrations following IP insulin bolus challenge, increased fasting serum insulin levels, and decreased GLUT4 mRNA expression in epididymal fat as compared with control mice (Figure 4C−E). Lymphatic ablation also resulted in increased mRNA expression of insulin receptor substrate (IRS), the adipogenesis regulators CCAAT/enhancer-binding protein alpha (C/EBP-α) and peroxisome proliferator-activated receptor gamma (PPAR-γ), leptin, and adiponectin in epididymal fat (Figure 4G−K). Finally, lymphatic ablation

also led to increased IRS-1 phosphorylation at S307 and higher HOMA-IR index scores (Figure 4F-L).

Consistent with the major role of lymphatic channels in cholesterol absorption and transport, lymphatic ablation resulted in lower serum levels of total cholesterol and HDL (Figure 4M−N). In contrast, confirming our hypothesis that lymphatic injury can alter systemic metabolism, this treatment resulted in significantly higher serum levels of total lipids, LDL, and triglycerides, as well as leptin, but had no effect on serum adiponectin (Figure 4O−R).

3.5. Mesenteric lymphatic injury causes adipose tissue inflammation

To determine how lymphatic ablation regulates inflammatory responses, and because obesity is characterized by low-grade chronic inflammation, we next analyzed the effects of lymphatic ablation on systemic inflammatory responses and changes in visceral adipose tissue (VAT), subcutaneous adipose tissue (SAT), and the liver. This treatment significantly increased serum and VAT concentrations of key inflammatory cytokines, including IFN-γ, TNF-α, IL-1β, and IL-6 (Figure 5A−B). In contrast, cytokine expression in SAT and the liver was largely unchanged, with only IL-6 protein increasing in SAT and TNF-α protein increased in the liver (Figure 5C−D). Taken together, our results suggest that intestinal lymphatic function, independent of obesity, regulates glucose and lipid metabolism, and that injury to the lymphatics results in inflammatory changes both systemically and in
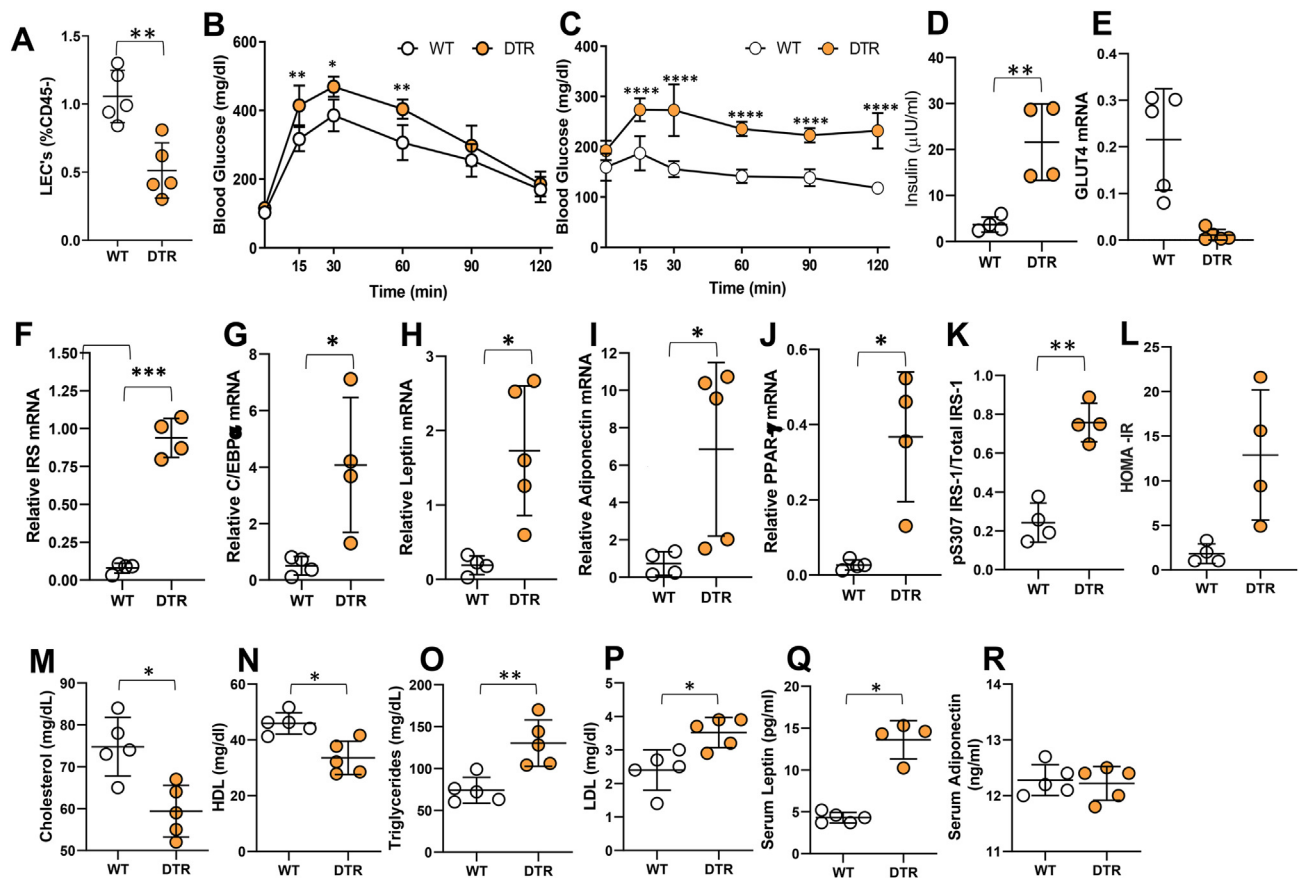
Figure 4: Lymphatic injury causes insulin resistance, dyslipidemia, and gene expression changes in adipose tissue. All panels compare WT and lymphatic-ablated (DT-treated [IP unless otherwise indicated] FLT4-cre$^{+/-}$-DTR$^{+/-}$) mice. (A) Quantification of LECs in intestinal tissue. Representative flow cytometry dot plots showing gating for CD45$^-$ CD31$^+$podoplanin$^+$ positive cells. (B—C) Tolerance of IP (B) glucose and (C) insulin. (D) Serum insulin. (E—J) qPCR-measured expression in epididymal fat of (E) the glucose transporter GLUT4, (F) IRS, (G) CCAAT/enhancer-binding protein alpha (C/EBP-α), (H) leptin, (I) adiponectin, and (J) peroxisome proliferator-activated receptor gamma (PPAR-γ). (K) ELISA-measured protein expression of phosphorylated IRS-1 (S307) relative to total IRS-1 in epididymal fat. (L) Insulin resistance calculated using homeostatic model assessment (HOMA-IR). (M—R) Serum lipid profiles of WT and FLT4-cre$^{+/-}$-DTR$^{+/-}$ mice for (M) total cholesterol, (N) HDL, (O) triglycerides, and (P) LDL. (Q—R) ELISA quantification of serum adipocytokines, (Q) leptin, and (R) adiponectin. N = 4—5/group, mean ± SD, unpaired Student t-test. (*P < 0.05, **P < 0.01, ***P < 0.001, ****P < 0.0001).

adipose tissues. Interestingly, despite the metabolic abnormalities noted in heterozygous FLT4-DTR mice 1 week after partial lymphatic ablation, we did not find any differences in their food intake, body weight, or reproductive fat pad (RFP) or inguinal fat pad weights (IFP) (Supplementary Figs. 6C—G). Furthermore, small intestine and liver histology showed no visible damage to both the tissues. With the exception of the dilation of the lamina propria lymphatic vessels, the morphology of the intestine and villi remain intact in heterozygous FLT4-DTR mice compared to controls (Supplementary Figs. 7A—B). Considering the glucose and metabolic abnormalities noted in the heterozygous FLT4-DTR mice, we performed liver function analysis to ensure normal liver functioning in these mice. Except for significantly elevated alkaline phosphatase (ALP), albumin heterozygous FLT4-DTR mice showed no differences in other enzymes, such as alanine transferase (ALT), aspartate transferase (AST), lactate dehydrogenase (LDH), total protein, globulins, bilirubin, and albumin-globulin ratio (A/G ratio) compared to controls (Supplementary Figure 7C-L).

3.6. Mesenteric lymphatic injury causes nitrosative stress in tissues

To understand the extent of lymphatic leakage caused by partial ablation of mesenteric lymphatic vessels in FLT4-DTR mice, we assessed lymphatic function by oral gavage of BODIPY cholesterol. The mesenteric lymphatics of DT-treated heterozygous FLT4-DTR mice were nearly 4 times more dilated and 2-fold leakier compared with wild-type controls (Figure 6A—C). To assess the contribution of iNOS to this dysfunction, we examined the co-localization of iNOS$^+$ cells and lymphatic vessels in mesenteric tissues using whole mount imaging and noted that, similar to our observations in obese mice, iNOS$^+$ cells tended to accumulate around lymphatics of DT-treated heterozygous FLT4-DTR mice (Figure 6D). Flow cytometry of mesenteric tissues revealed a nearly 3-fold increase in the number of iNOS$^+$ cells in lymphatic-ablated mice, corroborating our histological analysis (Figure 6E—F). We evaluated the effects of the resulting increased NO on mesenteric membranes by immunostaining for nitrotyrosine and found extensive tyrosine nitration in the peri-lymphatic mesothelium in DT-treated heterozygous FLT4-DTR mice (Figure 6G—H). Confirming these findings, we also observed increased peroxynitrite production in the mesenteric tissues by Griess reaction (Figure 6I).

To determine whether the metabolic abnormalities noted in DT-treated heterozygous FLT4-DTR mice are related to increased iNOS and the resulting reactive nitrogen species, we inhibited iNOS using 1400 W. As compared with control heterozygous FLT4-DTR lymphatic-ablated mice, inhibition of iNOS significantly improved insulin sensitivity as
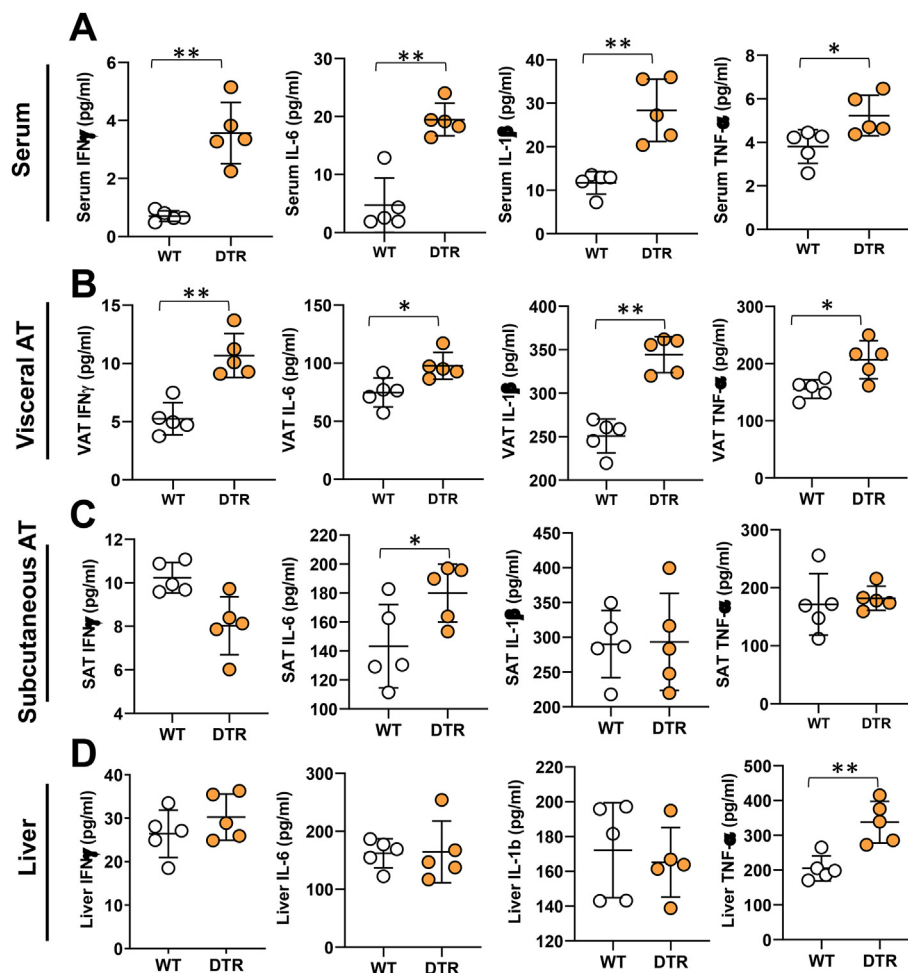
Figure 5: Lymphatic injury causes systemic and adipose tissue inflammation. All panels compare WT and lymphatic-ablated (DT-treated [IP unless otherwise indicated] FLT4-cre$^{+/-}$-DTR$^{+/-}$) mice. ELISA quantification of the inflammatory cytokines IFN-γ, IL-6, IL-1β, and TNF-α in (A) serum (B) visceral adipose tissue (VAT), (C) subcutaneous adipose tissue (SAT), and (D) liver. N = 5/group, mean ± SD, unpaired Student t-test. (*P < 0.05, **P < 0.01).

evidenced by decreased serum glucose levels 15 and 30 min after IP glucose challenge and decreased serum insulin levels (Figure 6J—K). Inhibition of iNOS also increased serum cholesterol to normal levels but did not significantly affect lipoprotein or triglyceride levels (Figure 6M—O).

4. DISCUSSION

In the current study, we show that obesity has significant pathologic effects on the lymphatic system and that this response is regulated, at least in part, by nitrosative stress-induced injury to LECs. In addition, and perhaps more importantly, we show that lymphatic injury alone can cause metabolic abnormalities, such as insulin resistance or dyslipidemia, and that changes in lymphatic function, independent of obesity or high-fat diets, can have significant effects on glucose and lipid metabolism. These findings suggest that treatments directed at preserving or improving lymphatic function may have a future role in managing metabolic abnormalities in obese individuals.

Given the important role of adipose tissues in glucose and lipid metabolism [42] in the current study, we investigated lymphatic function in the mesenteric white adipose tissues of obese wild-type and iNOS knockout mice. We show that these vessels are

dysfunctional, leaky, and display an abnormally dilated phenotype characteristic of loss of vessel tone [43], similar to our prior findings in the skin of obese mice [3]. Further, obese animals have significant accumulation of iNOS$^+$ CD45$^+$ inflammatory cells around mesenteric lymphatics [3]. These pathologic features are largely absent in obese iNOS knockout mice, suggesting that increased expression of iNOS plays a key role in the regulation of lymphatic dysfunction. Our findings are supported by other studies showing that iNOS contributes to lymphatic dysfunction in other inflammatory conditions, such as ileitis and arthritis [23,24,44,45].

We show that obesity significantly decreases mRNA expression of VEGFR-3 mRNA in mesenteric lymphatics, consistent with our previous findings in the subcutaneous lymphatics of obese mice [14]. VEFGR-3 signaling is an important regulator of LEC proliferation, migration, function, and survival *in vitro*. Recent reports also indicate that VEGFR-3 signaling is important for adult lymphatic maintenance; decreased ligand—receptor activity may decrease survival signals under normal or pathologic conditions in various tissues [46—49]. These findings are also interesting because VEGFR-3, like the insulin receptor, belongs to the tyrosine kinase family of growth factor receptors. Given that obesity is known to regulate glucose homeostasis by modulating insulin receptor expression and function, our findings suggest that impaired
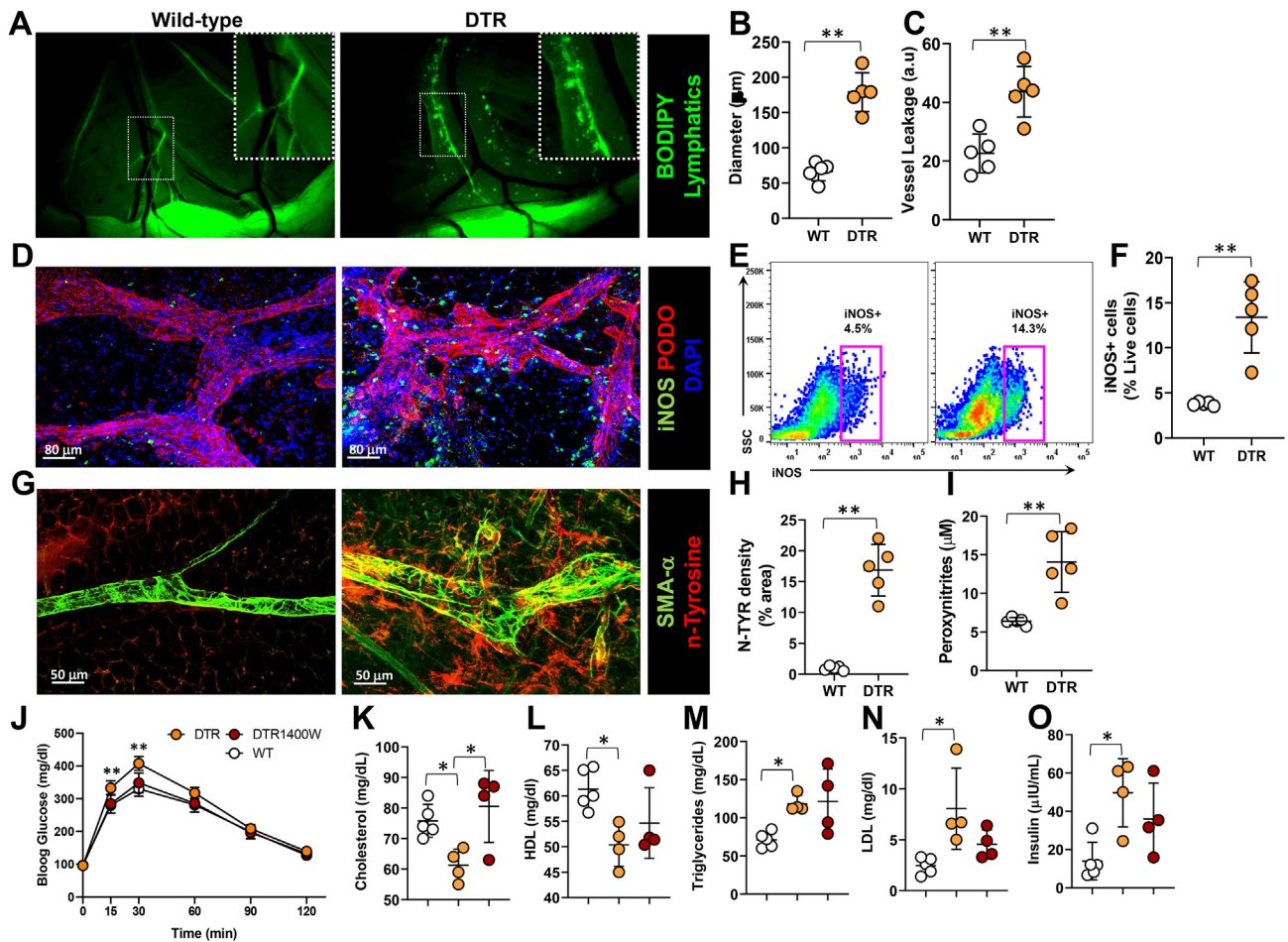
Figure 6: Lymphatic injury causes nitrosative stress in mesenteric tissues. A-I, WT vs. lymphatic-ablated (DT-treated [IP unless otherwise indicated] FLT4-cre$^{+/-}$-DTR$^{+/-}$) mice. (A) Visualization of collecting lymphatic vessels in mesenteric white adipose tissue (M-WAT) by oral gavage-administered BODIPY (FL-C16). Inset, 2x magnification showing dilated, leaky lymphatic vessels. Scale bar, 500 μm. (B) Quantification of M-WAT lymphatic vessel diameter and (C) BODIPY leakage into the extraluminal space. (D) Representative confocal microscopic images of whole mount M-WAT containing lymphatic vessels, immunostained for iNOS and podoplanin and counterstained with DAPI (scale bar, 80 μm). (E—F) Quantification of iNOS$^+$ cells in M-WAT; (E) representative flow cytometry dot plot and (F) as a percentage of live cells. (G) Representative confocal microscopic images of whole mount M-WAT containing lymphatic vessels, immunostained for alpha smooth muscle actin (α-SMA) and nitrosylated tyrosine (n-tyrosine) (scale bar, 50 μm). (H) Quantification of fluorescent n-tyrosine. (I) Peroxynitrite content in mesenteric tissues. J-O, comparison of WT and FLT4-cre$^{+/-}$-DTR$^{+/-}$ mice treated with 1400 W or vehicle (PBS). (J) Tolerance of IP-injected glucose bolus. (K—O) Serum lipid levels of (K) total cholesterol, (L) HDL (M) triglycerides, (N) LDL, and (O) serum insulin. N = 4—5; mean ± SD, two-way ANOVA with Sidak multiple comparison test or unpaired Student's *t*-test. (*P < 0.05, **P < 0.01, ***P < 0.001).

lymphatic function in obesity may be related, at least in part, to decreased sensitivity of LECs to VEGF-C survival signals as a result of decreased LEC VEGFR-3 expression. This hypothesis is supported by the fact that insulin-like growth factor (IGF-1), which is structurally homologous to insulin, can regulate LEC proliferation and function *in vitro* by activating Akt phosphorylation [50]. Although the mechanism by which obesity regulates VEGFR-3 expression is beyond the scope of this publication, such future investigations are crucial for fully understanding the regulation of lymphatic dysfunction in obesity.

We show that weight gain causes lymphatic injury by increasing accumulation of reactive nitrogen species and demonstrate that LECs are particularly sensitive to nitrosative stress in an irreversible manner. These findings agree with previous studies demonstrating that obesity markedly increases production of nitrogen and oxygen free radicals, and that systemic and adipose tissue nitrosative and oxidative stress are associated with metabolic dysfunction [51—53]. During obesity, free fatty acid-induced iNOS and oxidative stress reduce expression of antioxidant enzymes as well as insulin output by pancreatic beta cells,

resulting in diabetes; these effects are ameliorated by NO-lowering agents [53—55]. Similarly, we show that increased iNOS and reactive nitrogen species in obesity leads to reduced expression of antioxidant genes in LECs, thus rendering the highly oxidative stress-sensitive LECs dysfunctional [25,56].

Critically, we have shown that lymphatic injury independent of obesity leads to changes consistent with glucose intolerance and insulin resistance as observed in chronic obesity. These include increased fasting serum glucose and insulin and Homeostatic Model Assessment for Insulin Resistance (HOMA-IR), lowered expression of GLUT4, and increased IRS-1 phosphorylation and expression of many insulin-responsive genes in adipose tissue [57—62]. Inhibition of iNOS during lymphatic injury partially rescued glucose intolerance. Our results are consistent with previous studies demonstrating that mice with chronic lymphatic abnormalities resulting from haploinsufficiency of Prox-1, a master regulator of lymphatic differentiation, become obese as adults and have metabolic abnormalities even when fed a normal chow diet [4]. Thus, our study adds to the existing lymphatic literature

by showing that even short-term changes in lymphatic function can have significant effects on glucose and lipid metabolism.

5. CONCLUSIONS

Taken together, our findings support the hypothesis that obesity-induced lymphatic injury through elevated iNOS may act in a feed-forward manner to amplify the pathophysiology of obesity by regulating insulin sensitivity and promoting chronic inflammation. Thus, improving lymphatic function through modulation of iNOS and nitrative stress may represent a strategy to combat obesity-induced metabolic derangement.

ACKNOWLEDGMENTS

CONFLICT OF INTEREST

The authors declare that the research was conducted in the absence of any commercial or financial relationships that could be construed as a potential conflict of interest.

APPENDIX A. SUPPLEMENTARY DATA

Supplementary data to this article can be found online at https://doi.org/10.1016/j.molmet.2020.101081.

REFERENCES

[1] Blum, K.S., Karaman, S., Proulx, S.T., Ochsenbein, A.M., Luciani, P., Leroux, J.C., et al., 2014. Chronic high-fat diet impairs collecting lymphatic vessel function in mice. PLoS One 9(4):e94713.

[2] Savetsky, I.L., Torrisi, J.S., Cuzzone, D.A., Ghanta, S., Albano, N.J., Gardenier, J.C., et al., 2014. Obesity increases inflammation and impairs lymphatic function in a mouse model of lymphedema. American Journal of Physiology - Heart and Circulatory Physiology 307(2):H165—H172.

[3] Torrisi, J.S., Hespe, G.E., Cuzzone, D.A., Savetsky, I.L., Nitti, M.D., Gardenier, J.C., et al., 2016. Inhibition of inflammation and iNOS improves lymphatic function in obesity. Scientific Reports 6:19817.

[4] Escobedo, N., Proulx, S.T., Karaman, S., Dillard, M.E., Johnson, N., Detmar, M., et al., 2016. Restoration of lymphatic function rescues obesity in Prox1-haploinsufficient mice. JCI Insight 1(2).

[5] Harvey, N.L., Srinivasan, R.S., Dillard, M.E., Johnson, N.C., Witte, M.H., Boyd, K., et al., 2005. Lymphatic vascular defects promoted by Prox1 haploinsufficiency cause adult-onset obesity. Nature Genetics 37(10):1072—1081.

[6] Shew, T., Wolins, N.E., Cifarelli, V., 2018. VEGFR-3 signaling regulates triglyceride retention and absorption in the intestine. Frontiers in Physiology 9: 1783.

[7] Zhang, F., Zarkada, G., Han, J., Li, J., Dubrac, A., Ola, R., et al., 2018. Lacteal junction zippering protects against diet-induced obesity. Science 361(6402): 599—603.

[8] Chakraborty, S., Gurusamy, M., Zawieja, D.C., Muthuchamy, M., 2013. Lymphatic filariasis: perspectives on lymphatic remodeling and contractile dysfunction in filarial disease pathogenesis. Microcirculation 20(5):349—364.

[9] Dayan, J.H., Ly, C.L., Kataru, R.P., Mehrara, B.J., 2018. Lymphedema: pathogenesis and novel therapies. Annual Review of Medicine 69:263—276.

[10] Pond, C.M., Mattacks, C.A., 2002. The activation of the adipose tissue associated with lymph nodes during the early stages of an immune response. Cytokine 17(3):131—139.

[11] Rutkowski, J.M., Markhus, C.E., Gyenge, C.C., Alitalo, K., Wiig, H., Swartz, M.A., 2010. Dermal collagen and lipid deposition correlate with tissue swelling and hydraulic conductivity in murine primary lymphedema. American Journal Of Pathology 176(3):1122—1129.

[12] Greene, A.K., Maclellan, R.A., 2013. Obesity-induced upper extremity lymphedema. Plastic Reconstruction SurgeryGlobal Opening 1(7):e59.

[13] Arngrim, N., Simonsen, L., Holst, J.J., Bulow, J., 2013. Reduced adipose tissue lymphatic drainage of macromolecules in obese subjects: a possible link between obesity and local tissue inflammation? International Journal of Obesity 37(5):748—750.

[14] Nitti, M.D., Hespe, G.E., Kataru, R.P., Garcia Nores, G.D., Savetsky, I.L., Torrisi, J.S., et al., 2016. Obesity-induced lymphatic dysfunction is reversible with weight loss. Journal of Physiology 594(23):7073—7087.

[15] Hespe, G.E., Kataru, R.P., Savetsky, I.L., Garcia Nores, G.D., Torrisi, J.S., Nitti, M.D., et al., 2016. Exercise training improves obesity-related lymphatic dysfunction. Journal of Physiology 594(15):4267—4282.

[16] Sato, A., Kamekura, R., Kawata, K., Kawada, M., Jitsukawa, S., Yamashita, K., et al., 2016. Novel mechanisms of compromised lymphatic endothelial cell homeostasis in obesity: the role of leptin in lymphatic endothelial cell tube formation and proliferation. PLoS One 11(7):e0158408.

[17] Escobedo, N., Oliver, G., 2017. The lymphatic vasculature: its role in adipose metabolism and obesity. Cell Metabolism 26(4):598—609.

[18] Shimizu, Y., Shibata, R., Ishii, M., Ohashi, K., Kambara, T., Uemura, Y., et al., 2013. Adiponectin-mediated modulation of lymphatic vessel formation and lymphedema. Journal of American Heart Association 2(5):e000438.

[19] Gasheva, O.Y., Zawieja, D.C., Gashev, A.A., 2006. Contraction-initiated NO-dependent lymphatic relaxation: a self-regulatory mechanism in rat thoracic duct. Journal of Physiology 575(Pt 3):821—832.

[20] Gashev, A.A., Davis, M.J., Zawieja, D.C., 2002. Inhibition of the active lymph pump by flow in rat mesenteric lymphatics and thoracic duct. Journal of Physiology 540(Pt 3):1023—1037.

[21] Scallan, J.P., Davis, M.J., 2013. Genetic removal of basal nitric oxide enhances contractile activity in isolated murine collecting lymphatic vessels. Journal of Physiology 591(8):2139—2156.

[22] Scallan, J.P., Hill, M.A., Davis, M.J., 2015. Lymphatic vascular integrity is disrupted in type 2 diabetes due to impaired nitric oxide signalling. Cardiovascular Research 107(1):89—97.

[23] Chen, Y., Rehal, S., Roizes, S., Zhu, H.L., Cole, W.C., von der Weid, P.Y., 2017. The pro-inflammatory cytokine TNF-alpha inhibits lymphatic pumping via activation of the NF-kappaB-iNOS signaling pathway. Microcirculation 24(3).

[24] Mathias, R., von der Weid, P.Y., 2013. Involvement of the NO-cGMP-K(ATP) channel pathway in the mesenteric lymphatic pump dysfunction observed in the Guinea pig model of TNBS-induced ileitis. American Journal of Physiology - Gastrointestinal and Liver Physiology 304(6):G623—G634.

[25] Kasuya, A., Sakabe, J., Tokura, Y., 2014. Potential application of in vivo imaging of impaired lymphatic duct to evaluate the severity of pressure ulcer in mouse model. Scientific Reports 4:4173.

[26] Schulz, E., Gori, T., Munzel, T., 2011. Oxidative stress and endothelial dysfunction in hypertension. Hypertension Research 34(6):665—673.

[27] Martinez-Corral, I., Stanczuk, L., Frye, M., Ulvmar, M.H., Dieguez-Hurtado, R., Olmeda, D., et al., 2016. Vegfr3-CreER (T2) mouse, a new genetic tool for targeting the lymphatic system. Angiogenesis 19(3):433—445.

[28] Muniroh, M., Khan, N., Koriyama, C., Akiba, S., Vogel, C.F., Yamamoto, M., 2015. Suppression of methylmercury-induced IL-6 and MCP-1 expressions by N-acetylcysteine in U-87MG human astrocytoma cells. Life Sciences 134: 16—21.

MOLECULAR METABOLISM 42 (2020) 101081 11
www.molecularmetabolism.com

Original Article

[29] Pieralisi, A., Martini, C., Soto, D., Vila, M.C., Calvo, J.C., Guerra, L.N., 2016. N-acetylcysteine inhibits lipid accumulation in mouse embryonic adipocytes. Redox Biology 9:39—44.

[30] Vezir, O., Comelekoglu, U., Sucu, N., Yalin, A.E., Yilmaz, S.N., Yalin, S., et al., 2017. N-Acetylcysteine-induced vasodilatation is modulated by KATP channels, Na(+)/K(+)-ATPase activity and intracellular calcium concentration: an in vitro study. Pharmacological Reports 69(4):738—745.

[31] Green, L.C., Wagner, D.A., Glogowski, J., Skipper, P.L., Wishnok, J.S., Tannenbaum, S.R., 1982. Analysis of nitrate, nitrite, and [15N]nitrate in biological fluids. Analytical Biochemistry 126(1):131—138.

[32] Matthews, D.R., Hosker, J.P., Rudenski, A.S., Naylor, B.A., Treacher, D.F., Turner, R.C., 1985. Homeostasis model assessment: insulin resistance and beta-cell function from fasting plasma glucose and insulin concentrations in man. Diabetologia 28(7):412—419.

[33] Perreault, M., Marette, A., 2001. Targeted disruption of inducible nitric oxide synthase protects against obesity-linked insulin resistance in muscle. Nature Medicine 7(10):1138—1143.

[34] Soskic, S.S., Dobutovic, B.D., Sudar, E.M., Obradovic, M.M., Nikolic, D.M., Djordjevic, J.D., et al., 2011. Regulation of inducible nitric oxide synthase (iNOS) and its potential role in insulin resistance, diabetes and heart failure. The Open Cardiovascular Medicine Journal 5:153—163.

[35] Wiseman, D.A., Thurmond, D.C., 2012. The good and bad effects of cysteine S-nitrosylation and tyrosine nitration upon insulin exocytosis: a balancing act. Current Diabetes Reviews 8(4):303—315.

[36] Bartesaghi, S., Radi, R., 2018. Fundamentals on the biochemistry of peroxynitrite and protein tyrosine nitration. Redox Biology 14:618—625.

[37] MacMillan-Crow, L.A., Crow, J.P., Kerby, J.D., Beckman, J.S., Thompson, J.A., 1996. Nitration and inactivation of manganese superoxide dismutase in chronic rejection of human renal allografts. Proceedings of the National Academy of Sciences of the United States of America 93(21):11853—11858.

[38] Cerutti, P., Larsson, R., Krupitza, G., Muehlematter, D., Crawford, D., Amstad, P., 1989. Pathophysiological mechanisms of active oxygen. Mutation Research 214(1):81—88.

[39] Gardenier, J.C., Hespe, G.E., Kataru, R.P., Savetsky, I.L., Torrisi, J.S., Nores, G.D.G., et al., 2016. Diphtheria toxin-mediated ablation of lymphatic endothelial cells results in progressive lymphedema. JCI Insight 1(15):e84095.

[40] Kaipainen, A., Korhonen, J., Mustonen, T., van Hinsbergh, V.W., Fang, G.H., Dumont, D., et al., 1995. Expression of the fms-like tyrosine kinase 4 gene becomes restricted to lymphatic endothelium during development. Proceedings of the National Academy of Sciences of the United States of America 92(8):3566—3570.

[41] Hamrah, P., Chen, L., Zhang, Q., Dana, M.R., 2003. Novel expression of vascular endothelial growth factor receptor (VEGFR)-3 and VEGF-C on corneal dendritic cells. American Journal Of Pathology 163(1):57—68.

[42] Rosen, E.D., Spiegelman, B.M., 2006. Adipocytes as regulators of energy balance and glucose homeostasis. Nature 444(7121):847—853.

[43] Benoit, J.N., 1997. Effects of alpha-adrenergic stimuli on mesenteric collecting lymphatics in the rat. American Journal of Physiology 273(1 Pt 2):R331—R336.

[44] Liao, S., Cheng, G., Conner, D.A., Huang, Y., Kucherlapati, R.S., Munn, L.L., et al., 2011. Impaired lymphatic contraction associated with immunosuppression. Proceedings of the National Academy of Sciences of the United States of America 108(46):18784—18789.

[45] Liang, Q., Ju, Y., Chen, Y., Wang, W., Li, J., Zhang, L., et al., 2016. Lymphatic endothelial cells efferent to inflamed joints produce iNOS and inhibit lymphatic vessel contraction and drainage in TNF-induced arthritis in mice. Arthritis Research and Therapy 18:62.

[46] Coso, S., Bovay, E., Petrova, T.V., 2014. Pressing the right buttons: signaling in lymphangiogenesis. Blood 123(17):2614—2624.

[47] Dumont, D.J., Jussila, L., Taipale, J., Lymboussaki, A., Mustonen, T., Pajusola, K., et al., 1998. Cardiovascular failure in mouse embryos deficient in VEGF receptor-3. Science 282(5390):946—949.

[48] Nurmi, H., Saharinen, P., Zarkada, G., Zheng, W., Robciuc, M.R., Alitalo, K., 2015. VEGF-C is required for intestinal lymphatic vessel maintenance and lipid absorption. EMBO Molecular Medicine 7(11):1418—1425.

[49] Zarkada, G., Heinolainen, K., Makinen, T., Kubota, Y., Alitalo, K., 2015. VEGFR3 does not sustain retinal angiogenesis without VEGFR2. Proceedings of the National Academy of Sciences of the United States of America 112(3):761—766.

[50] Bjorndahl, M., Cao, R., Nissen, L.J., Clasper, S., Johnson, L.A., Xue, Y., et al., 2005. Insulin-like growth factors 1 and 2 induce lymphangiogenesis in vivo. Proceedings of the National Academy of Sciences of the United States of America 102(43):15593—15598.

[51] Jankovic, A., Korac, A., Buzadzic, B., Stancic, A., Otasevic, V., Ferdinandy, P., et al., 2017. Targeting the NO/superoxide ratio in adipose tissue: relevance to obesity and diabetes management. British Journal of Pharmacology 174(12):1570—1590.

[52] Morelli, N.R., Scavuzzi, B.M., Miglioranza, L., Lozovoy, M.A.B., Simao, A.N.C., Dichi, I., 2018. Metabolic syndrome components are associated with oxidative stress in overweight and obese patients. Archives in Endocrinology Metabolism 62(3):309—318.

[53] Shimabukuro, M., Ohneda, M., Lee, Y., Unger, R.H., 1997. Role of nitric oxide in obesity-induced beta cell disease. Journal of Clinical Investigation 100(2):290—295.

[54] Wang, J., Wang, H., 2017. Oxidative stress in pancreatic beta cell regeneration. Oxidative Medical Cell Longev 2017:1930261.

[55] Gerber, P.A., Rutter, G.A., 2017. The role of oxidative stress and hypoxia in pancreatic beta-cell dysfunction in diabetes mellitus. Antioxidants and Redox Signaling 26(10):501—518.

[56] Zawieja, D.C., Greiner, S.T., Davis, K.L., Hinds, W.M., Granger, H.J., 1991. Reactive oxygen metabolites inhibit spontaneous lymphatic contractions. American Journal of Physiology 260(6 Pt 2):H1935—H1943.

[57] MacLaren, R., Cui, W., Simard, S., Cianflone, K., 2008. Influence of obesity and insulin sensitivity on insulin signaling genes in human omental and subcutaneous adipose tissue. The Journal of Lipid Research 49(2):308—323.

[58] Wrann, C.D., Rosen, E.D., 2012. New insights into adipocyte-specific leptin gene expression. Adipocyte 1(3):168—172.

[59] Vidal-Puig, A., Jimenez-Linan, M., Lowell, B.B., Hamann, A., Hu, E., Spiegelman, B., et al., 1996. Regulation of PPAR gamma gene expression by nutrition and obesity in rodents. Journal of Clinical Investigation 97(11):2553—2561.

[60] Rolland, V., Le Liepvre, X., Houbiguian, M.L., Lavau, M., Dugail, I., 1995. C/EBP alpha expression in adipose tissue of genetically obese Zucker rats. Biochemical and Biophysical Research Communications 207(2):761—767.

[61] Poletto, A.C., David-Silva, A., Yamamoto, A.P., Machado, U.F., Furuya, D.T., 2015. Reduced Slc2a4/GLUT4 expression in subcutaneous adipose tissue of monosodium glutamate obese mice is recovered after atorvastatin treatment. Diabetology & Metabolic Syndrome 7:18.

[62] Peng, J., He, L., 2018. IRS posttranslational modifications in regulating insulin signaling. Journal of Molecular Endocrinology 60(1):R1—R8.